Soft Matter

PAPER

Cite this: *Soft Matter*, 2015, **11**, 2806

Temperature dependent coordinating self-assembly

Yijie Wang,†[a] Xuedong Gao,†[a] Yunlong Xiao,[b] Qiang Zhao,[a] Jiang Yang,[c] Yun Yan*[a] and Jianbin Huang*[a]

Received 8th December 2014
Accepted 10th February 2015

DOI: 10.1039/c4sm02717e

www.rsc.org/softmatter

Self-assemblies dominated by coordination interaction are hardly responsive to thermal stimuli. We show that in case the coordinating mode changes with temperature, the resultant assemblies also exhibit temperature dependence. The self-assemblies are constructed with perylene tetracarboxylate and metal ions. Compounds containing a perylene skeleton often self-assemble into micro-belts, which is also true for the combination of perylene tetracarboxylate and metal ions. However, a unique pinecone structure was observed upon increasing the temperature of the coordinating system. The structural transition is triggered by the change of coordinating mode between the carboxylate group and the metal ion. At low temperature, intermolecular coordination occurs which favours the growth of the coordinating self-assembly along the long axis of the perylene. However, upon the elevation of temperature, the coordination is overwhelmed by intra-molecular mode. This is against the extension of the coordinating assembly due to the loss of connection between neighbouring perylenes. As a result, the pinecone structure is observed. We expect that the cases introduced in this work may inspire the design of structurally controllable temperature-dependent soft materials based on coordinating self-assembly.

Introduction

Coordinating interaction has gained an enormous amount of interest in the field of self-assembly since it provides directional noncovalent force that drives coordinating molecules to assemble into desired structures. Despite the earliest studies of various metal–organic frameworks (MOFs),[1–3] it was found that coordinating interaction may trigger a large variety of molecules to assemble into amazing soft materials. Excellent examples include various metallo supramolecular polymers,[4–12] the metal mediated self-assembly of amphiphilic molecules,[13–18] nanometer sized coordination polymers,[19–25] *etc.* Different from other weak noncovalent interactions, such as the hydrophobic effect,[26] hydrogen bonding,[27,28] van der Waals forces,[29] or π–π stacking,[30,31] coordination force[32,33] is very strong and in some cases may be comparable to some covalent bonds. For this reason, many metallic elements were incorporated into the main or side chain of polymers simply *via* coordination interaction to form robust materials.[21,22] On the other hand, the extremely strong coordination tendency makes the self-assembled structures dominated by coordination interaction difficult to respond to external stimuli. This greatly minimized their advantages as soft materials which normally exhibit structural and practical flexibility. Although there are some successful cases in this regard,[8,11] it is still a challenging work to find more cases and to get a general approach to create temperature sensitive coordinating self-assembly.

Actually, coordination interaction can be greatly affected by temperature. For instance, recently Szczerba *et al.*[10] found that the film of MEPEs exhibited temperature sensitive colour change. This was attributed to the torsion of the crystal field, which indicates that the coordinating bond indeed exhibits noncovalent nature which is responsive to temperature. However, temperature responsiveness may not be observed in many cases because the change of the coordinating state is not strong enough to influence the molecular packing. This inspires that if the contribution of coordination is increased in a coordinating self-assembly, the change in the coordinating states may lead to a considerable self-assembly change.

Herein we report that the coordinating self-assembly of perylene tetracarboxylate (PTC) and metal ions (M) indeed exhibits thermal sensitive structures. The PTC ion contains 4 carboxyl groups, each of which may coordinate with one metal ion. The coordinating effect in this system is very significant. It is well-known that perylene backbones have a strong tendency to stack *via* the π–π interaction owing to their planar aromatic structures.[34–38] If there are no structural limitations, the stacking

[a]*Beijing National Laboratory for Molecular Sciences (BNLMS), State Key Laboratory for Structural Chemistry of Unstable and Stable Species, College of Chemistry and Molecular Engineering, Peking University, Beijing 100871, P. R. China. E-mail: yunyan@pku.edu.cn; jbhuang@pku.edu.cn*

[b]*Institute of Theoretical and Computational Chemistry, College of Chemistry and Molecular Engineering, Peking University, Beijing 100871, P. R. China*

[c]*Department of Petroleum Engineering, China University of Petroleum, Qingdao, Shandong, P. R. China*

† These authors equally contributed to this work.

of the aromatic skeleton often leads to plate-like structures.[37] However, in the presence of side chains or other steric constraints, stacking of the aromatic portion is restricted into one-dimension, which often leads to fibers or belts.[35,36] The PTC ion studied in this work itself does not self-assemble due to the presence of four carboxylate ions on the skeleton. We expect that coordinating self-assembly may occur upon addition of metal ions. Because the contribution of coordination interaction is very significant for the self-assembly formation, change of the coordinating state will influence the stacking of the PTC skeleton, which further affects the self-assembled structure.

In this work we show that the PTC–M coordinating systems, where the metal ions (M) can be Ni^{2+}/Ca^{2+}/Zn^{2+}/Cu^{2+}, *etc.*, may self-assemble into a micro-belt at room temperature, but into a pinecone upon elevating the temperature. Theoretical analysis and further experiments suggest that binding of metal ions with the carboxylate group at low temperature is intermolecular bidentate chelation, which facilitates the growth of the coordinating self-assembly along the long axis of PTC. However, in this coordinating state the plane of PTC is distorted so that the energy is high. In contrast, upon increasing the temperature, the coordination between the carboxylate ions and the metal ions becomes intramolecular bidentate chelation, which reduces the distortion tension of the PTC plane thus bringing the system to a low energy state. Because this intramolecular coordination leads to separate a coordinating unit, bond connection with the neighbouring coordinating unit is lost. This is against the growth of the coordinating self-assembly along the long axis of the PTC. As a result, pinecones are formed finally. This is for the first time it has been demonstrated that temperature-responsive coordinating mode has resulted in different self-assembled structures, which may inspire new designs and applications of coordinating self-assembly in the field of soft materials.

Experimental

Materials

3,4,9,10-Perylenetetracarboxylic dianhydride (PTCDA) was purchased from Alfa Aesar. Metal nitrates and other chemicals were purchased from Beijing Chemical Company. All chemicals were of analytical grade and were used as received. The tetrapotassium salt of 3,4,9,10-perylenetetracarboxylic acid (K_4PTC) was synthesized as previously reported.[39] 1.175 g PTCDA (3 mmol) was dissolved in 50 mL KOH aqueous solution (0.4 M) under stirring at 80 °C for 3 h. After cooling to room temperature, the mixture was filtered and 45 mL ethanol was added to the filtrate. The solid precipitated from the solution was filtered, washed with ethanol, and recrystallized with H_2O/ethanol (6/5 v/v) to give an orange crystal of $K_4PTC \cdot 4H_2O$ (yield 85%). ^{1}H NMR (400 MHz, D_2O): δ = 8.43 (d, 4H), 7.82 (d, 4H) ppm; elemental analysis: calcd (%) for $K_4PTC \cdot 4H_2O$: C 44.16, H 2.47; found: C 44.45 and H 2.58.

Preparation of PTC–M assemblies

The PTC–M micro-belts were obtained by directly vortex mixing K_4PTC solution with metal nitrate solution. In a typical procedure, the stock solutions of 2 mM K_4PTC and 4 mM nickel nitrate were mixed in a volume ratio of 1 : 1 and the resulting mixture of 1 mM PTC/2 mM Ni(II) was kept at 25 °C in an incubator for 24 h. The needle crystals formed during this process were then collected by centrifugation, washed with ethanol, and dispersed into ethanol solution.

Characterization

The scanning electron microscopy (SEM) and energy-dispersive spectroscopy (EDS) measurements were performed on a Hitachi S4800 microscope. Transmission electron microscopy (TEM) images and selected-area electron diffraction (SAED) spectra were recorded with a JEM-2100 instrument at an acceleration voltage of 200 kV. For SEM and TEM measurements, a drop of suspension (PTC–M assemblies dispersed into ethanol) was placed on clean silicon sheets or carbon-coated copper grids and dried in the air. Powder X-ray diffraction (XRD) patterns were measured using a Rigaku Dmax-2400 diffractometer with Cu Kα radiation. The samples (several drops of the suspension) were air-dried on clean glass slides. Ultraviolet-visible (UV-vis) spectral measurements were performed on a Shimadzu UV-1800 spectrophotometer. Fluorescence (FL) measurements were carried out using a Hitachi F-4500 instrument. The ethanol suspensions were used directly for UV-vis and FL measurements. Fourier transform infrared (FT-IR) spectra were recorded with a Bruker Vector-22 spectrophotometer and dry powders of the samples were examined using the KBr pressed pellet method.

Theoretical calculation

The coordinating modes and the corresponding energies were calculated at the restricted density functional theory level. The hybrid functional B3LYP and the 6-311+g(d,p) basis set were used. All calculations were performed using the Gaussian09 package. In order to decrease the difficulty of calculation, Ca^{2+} was chosen as the representing model metal ion in the calculations.

Results and discussion

PTC (Fig. 1a) exhibits very good solubility (up to 20 mM) in water owing to the presence of four negative charges carried by the tetracarboxylate ions. Upon addition of 2 mM $Ni(NO_3)_2$ into the 1 mM PTC solution, slow precipitation occurs, suggesting the formation of coordinating self-assembly. Orange-coloured needle-like crystals with lengths in the range of millimeters (Fig. 1b) were observed after the mixture was incubated at 25 °C for 12 h. SEM measurement reveals the microscopic feature of the crystals being ultralong micro-belts with a thickness of 100–300 nm and a width of 0.5–2.5 μm (Fig. 1b–d). This belt structure is typical for perylene derivatives, indicating strong π–π stacking that has occurred in the self-assembling process. However, if the coordinating system was incubated at 60 °C for 12 h, pinecone-shaped structures with diameters of 1–3 μm were obtained (Fig. 1e). More careful observations demonstrate

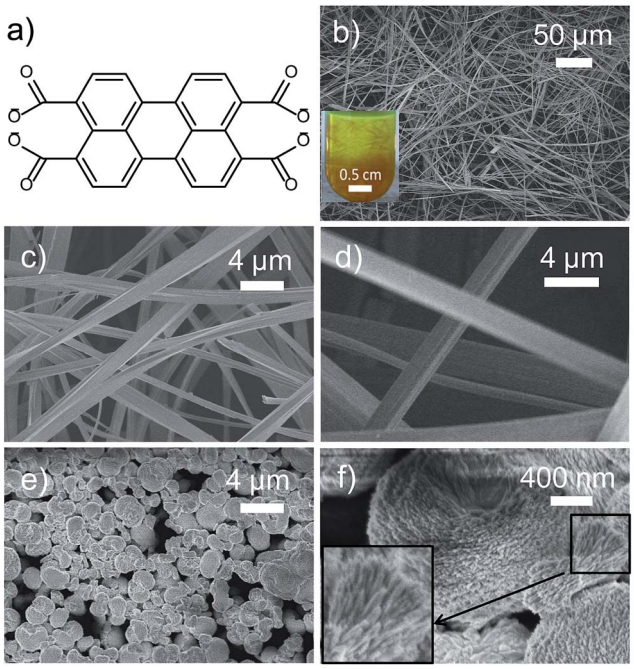

Fig. 1 (a) Scheme of the chemical structure of the perylene tetracarboxylate ion (PTC). SEM images of micro-belts (b–d) from a 1 mM PTC/2 mM Ni(II) mixture incubated at 25 °C for 24 h, and (e and f) pinecone structures from a 1 mM PTC/2 mM Ni(II) mixture incubated at 60 °C for 24 h. The inset in (b) and (f) are the photos of the yellow precipitates and the enlarged view of the selected section, respectively.

that the pinecone structure is hierarchical and composed of abundant nanorods (Fig. 1f).

In order to gain more physical insight into the structural transition at molecular level, XRD measurements were performed for the micro-belt and the pinecone, respectively. A dramatic difference on the diffraction patterns was observed for these two different structures. Fig. 2 shows that the belt displays fewer peaks than the pinecones. Three main peaks located at $2\theta = 6.8°$, 12.1° and 26.2° were observed for the micro-belts, corresponding to the d values of 1.30, 0.74 and 0.34 nm. The distances of 1.30 and 0.74 nm are closer to the length (1.11 nm) and width (0.68 nm) of PTC, respectively, whereas the d-spacing of 0.34 nm is characteristic of the π–π stacking.[40] These results indicate that the co-facial stacking of PTC groups has occurred in the PTC–Ni micro-belts. In contrast, 6 diffraction peaks are discernible for the pinecones, indicating that the periodical nature in the pinecones is more significant. It is worth noting that the first peak is extremely sharp in comparison with that in the micro-belt, suggesting that the lattice period which is characteristic of the length of PTC is very much strengthened in the pinecones. Further explanation of this sharp diffraction can be found later in the text after Fig. 5. Anyway, the XRD patterns in Fig. 2 strongly indicate a different molecular packing in the pinecones from that in the micro-belts.

The different molecular packing states in the micro-belts and pinecones are also reflected in the UV-vis and fluorescence spectra. The absorption spectrum of dilute K_4PTC solution shows two pronounced peaks at 467 and 438 nm and two shoulders around 412 and 385 nm (Fig. 3a), corresponding to the 0–0, 0–1, 0–2 and 0–3 electronic transitions, respectively.[41]

Upon formation of the PTC–Ni(II) micro-belts, the absorption peaks are obviously broadened and red-shifted to 492, 460, 424 and 404 nm. Moreover, a new band emerges at about 555 nm. The red-shift and line broadening of the four peaks are attributed to the delocalization of electrons in the excited state due to the intermolecular electronic interactions of the close-packed molecules,[42,43] whereas the new band emerging at a longer wavelength is a typical sign of the effective π–π interaction in the co-facial configuration.[41,44] In analogy, the absorption peaks for the PTC–Ni(II) pinecones also show red-shifts and line broadening, but the peaks are sharper and shift to much longer waves. This indicates that the energy levels in the pinecones are more distinct and the extent of delocalization of electrons is increased.

Since the π–π stacking can hardly be affected by temperature, the temperature dependent structure in the PTC–Ni system is expected to be triggered by the change of coordination states with increasing temperature. In order to understand the coordinating state at different temperatures, FT-IR measurements were performed for the micro-belts and pinecones (Fig. 4) in the PTC–Ni system. Usually, carboxylate acid displays a single band around 1700 cm^{-1} that arose from the

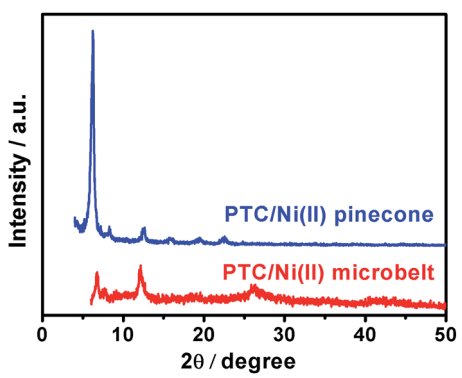

Fig. 2 XRD pattern of the PTC–Ni(II) microbelts (red line) and pinecone structures (blue line).

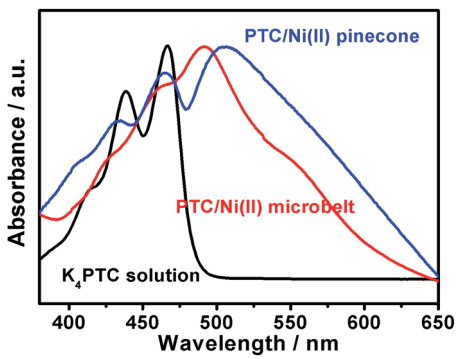

Fig. 3 UV-vis spectra of a 40 μM K_4PTC solution (black line) and of the PTC–Ni(II) micro-belts (red line) and pinecone structures (blue line) dispersed in ethanol.

antisymmetric C=O stretching vibration. Upon coordinating with metal ions, this single band splits into doublet ones, corresponding to the asymmetric and symmetric stretching vibration of C=O, respectively.[15] The frequency separation $\Delta\nu = \nu_{as(COO)} - \nu_{s(COO)}$ characterizes different coordinating modes between the metal ions and the carboxyl groups.[45,46] Monodentate, bidentate bridging, and bidentate chelating correspond to $\Delta\nu$ values much larger, approximately equal, and much smaller than 200 cm^{-1}, respectively. Fig. 4 shows that the $\Delta\nu$ for both the PTC–Ni(II) micro-belts (128 cm^{-1}) and pinecones (111 cm^{-1}) are far less than 200 cm^{-1}, strongly suggesting bidentate chelating coordination in both structures. However, the smaller $\Delta\nu$ in the pinecones indicates that the coordinating field of the pinecones is more symmetric than that of the micro-belts.

Elemental analysis results suggested similar PTC–Ni molar ratios in the micro-belts and pinecones (data not shown). This means that the two coordinating states corresponding to the two distinctly different coordinating assemblies are structural isomers. In combination of all these information and with the help of theoretical calculation, we infer that inter- and intra-molecular coordination may be the origin of the different structures. At low temperatures, the thermal motion of PTC and the metal ion is slow and strong electrostatic interaction drives the formation of intermolecular coordination, as illustrated in Fig. 5a. This is because electrostatic interaction occurs immediately upon addition of metal ions into the aqueous solution of PTC. Charge balance requires that one divalent metal ion attracts two carboxylate ions. If the two carboxylate ions come from two PTC (Fig. 5a), less steric hindrance is encountered. This simultaneously leads to the formation of one-dimensional coordinating chains (Fig. 5a). π–π stacking of such chains may result in micro-belts. However, this inter-molecular coordination also results in distortion of the PTC plane (Fig. 5b), so that the system tends to release this tension to form a more planar configuration. Restricted density functional calculation suggests that intramolecular coordination (Fig. 5c and d) may reduce the distortion and the energy of the coordinating system can be decreased by a value of 156.88 kcal mol^{-1}. The side view of the two coordinating modes in Fig. 5b and d clearly shows that the PTC skeleton in the form of intramolecular coordination is closer to a plane than its intermolecular counterpart. However, in the case of intramolecular coordination, the bond connection between neighbouring PTC–M is missing, which is not favourable to self-assemble along the long axis of the PTC. This means that although intramolecular coordination is

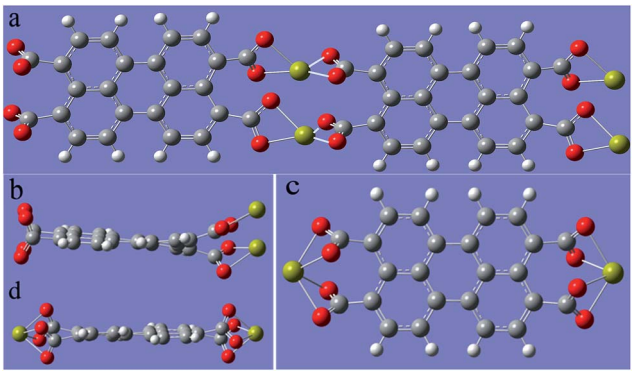

Fig. 5 Molecular modelling of the coordinating states between PTC and the metal ion. (a and b) are the front and side views of the inter-molecular coordinating PTC–M system; (c and d) are for the intra-molecular coordination.

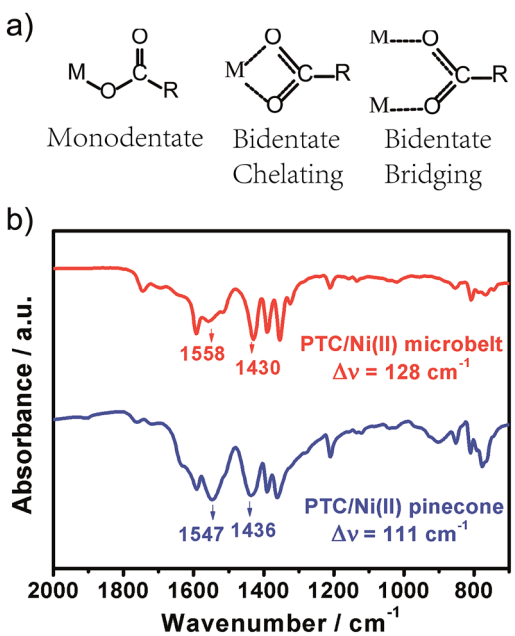

Fig. 4 (a) Three carboxylate coordination modes. (b) FT-IR spectra of PTC–Ni(II) micro-belts (red line) and PTC–Ni(II) pinecone structures (blue line).

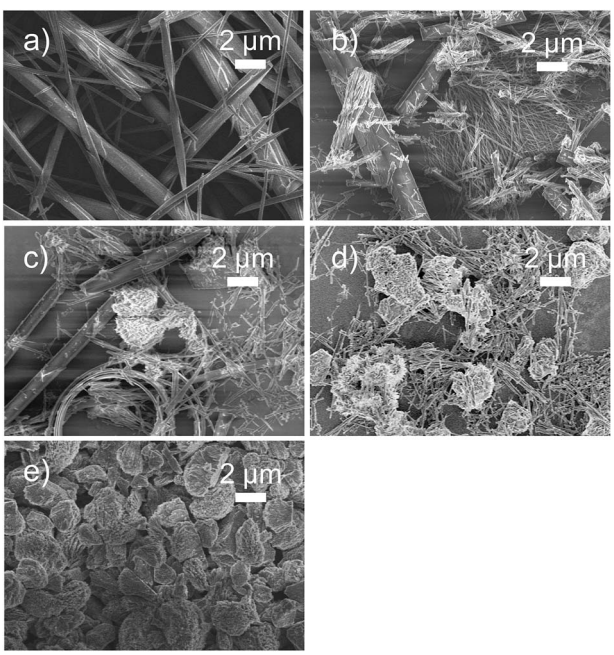

Fig. 6 Transformation of the self-assembled structures in the PTC–Ni system incubated at 40 °C. (a to e) Corresponds to the incubating time of 10 min, 2 h, 6 h, 12 h, and 24 h, respectively.

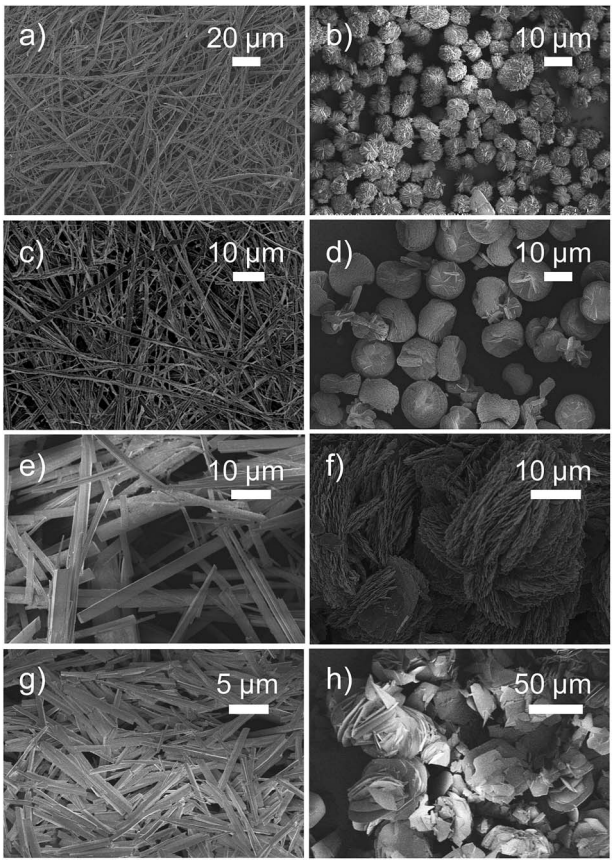

Fig. 7 SEM images of (a and b) micro-belts and pinecone structures from the PTC/Ca(II) (1 mM/2 mM) system incubated at 4 °C for 2 h and for 24 h, respectively, (c and d) micro-belts and pinecone structures from the PTC/Co(II) (1 mM/2 mM) system incubated for 12 h at 4 °C and 25 °C, respectively, (e and f) micro-belts and pinecone structures from the PTC/Cd(II) (1 mM/2 mM) system incubated for 8 h at 4 °C and 25 °C, respectively, and (g and h) micro-belts and pinecone structures from the PTC/Zn(II) (0.25 mM/0.5 mM) system incubated for 8 h at 4 °C and 25 °C, respectively.

thermodynamically favourable, it lacks the driving force to grow into micro-belts. That is why they form short nanorods, which further assemble into pinecones.

The better planar conformation of PTC in the pinecones than in the micro-belts leads to a better stacking of the PTC plane in the former, which explains the observation of more peaks in the XRD pattern and the longer waves in the UV spectra in the pinecones. It is possible that the planar independent intramolecular coordinating unit as illustrated in Fig. 5c (or d) is the distinct building block of the nanorods in the pinecones. As a result, the periodical nature of the length of this block is very intensive, which thus displays extremely sharp diffraction peaks in the XRD measurement in Fig. 2. Meanwhile, the better planar conformation like Fig. 5d also results in a more symmetric molecular environment than the distorted one (Fig. 5b), which is in accordance with the smaller $\Delta\nu$ of the carboxyl group in the IR of the pinecones.

It is noteworthy that migration of the metal ion is required in this proposed model. This means that the structural transition from micro-belts to pinecones must occur in solution because the solvent may act as the medium of mass transfer. Excitingly, we indeed found that the structural transformation occurred only when the micro-belts were left with water. The dried belts would never transform into pinecones. This confirms that the solution mediated equilibrium is very crucial in the structural change. However, once the pinecones were formed, reverse transformation of belts would not occur, which means that the pinecone structures are the energy-favourable state. This is in good accordance with the theoretical calculations.

The thermal dynamic favourable nature of the pinecones can be further confirmed by the time-dependent structure transformation at 40 °C. Fig. 6 shows that micro-belts were formed initially (Fig. 6a), but structural diversity already occurs after the belts were incubated for 2 hours. A few pinecones were observed within 6 hours, and the system was dominated by pinecones within 24 hours. Compared with those prepared at 60 °C within the same period (Fig. 1e and f), these pinecones are not well-defined. This unambiguously proved that the temperature triggered transformation from micro-belts to pinecones is a result of the energy competitive self-assembly. Increasing temperature helps to overcome the potential barrier between the inter- and intra-molecular coordinating modes, where the latter is a lower energy state.

The transition mechanism indicates that such a transformation process would be general for other metal ions. Similar structural transitions were indeed observed when Ni^{2+} was replaced with Ca, Cd, Zn, Co, *etc.* (Fig. 7), only that the reacting temperature or incubating period is different. For instance, structural transition in PTC/Ca(II) and PTC/Co(II) systems occurred just at 4 °C. It is possible that the different metal–ligand coordination details lead to lower energy barriers in the PTC/Ca(II) and PTC/Co(II) systems.

Conclusions

In conclusion, coordinating self-assemblies in PTC–M systems can be made thermally responsive by utilizing the temperature dependent coordination between metal ions and carboxylate groups. At low temperature, electrostatic interaction drives the formation of intermolecular coordination, which results in the one-dimensional growth of the self-assembly to form micro-belts. Because the intermolecular coordination results in the distortion of the PTC skeleton, the micro-belts are in a high energy state. Increasing temperature helps to reassemble the system into intramolecular coordination which reduces the distortion of the PTC plane. This leads to a better periodical stacking of PTC molecules and brings the system to a lower-energy state. However, the intramolecular coordination cut-off the connection between two neighbouring PTC which disfavours the one-dimensional growth of the self-assembly and results in the formation of pinecones. The transformation from micro-belts to pinecones is the result of the conversion from intermolecular coordination to intramolecular coordination. This mechanism may inspire designs of structurally controllable temperature-dependent soft materials based on coordinating self-assembly.

Acknowledgements

This work was supported by the National Natural Science Foundation of China (21273013, 21173011, 21422302, 21473005,51174163), and National Basic Research Program of China (973 Program, 2013CB933800).

Notes and references

1 S. L. James, *Chem. Soc. Rev.*, 2003, **32**, 276–288.
2 J. Lee, O. K. Farha, J. Roberts, K. A. Scheidt, S. T. Nguyen and J. T. Hupp, *Chem. Soc. Rev.*, 2009, **38**, 1450–1459.
3 L. E. Kreno, K. Leong, O. K. Farha, M. Allendorf, R. P. Van Duyne and J. T. Hupp, *Chem. Rev.*, 2012, **112**, 1105–1125.
4 J. B. Beck and S. J. Rowan, *J. Am. Chem. Soc.*, 2003, **125**, 13922–13923.
5 O. M. Yaghi, M. O'Keeffe, N. W. Ockwig, H. K. Chae, M. Eddaoudi and J. Kim, *Nature*, 2003, **423**, 705–714.
6 J. B. Beck, J. M. Ineman and S. J. Rowan, *Macromolecules*, 2005, **38**, 5060–5068.
7 W. G. Weng, J. B. Beck, A. M. Jamieson and S. J. Rowan, *J. Am. Chem. Soc.*, 2006, **128**, 11663–11672.
8 S. Y. Zhang, S. J. Yang, J. B. Lan, Y. R. Tang, Y. Xue and J. S. You, *J. Am. Chem. Soc.*, 2009, **131**, 1689–1691.
9 R. Chakrabarty, P. S. Mukherjee and P. J. Stang, *Chem. Rev.*, 2011, **111**, 6810–6918.
10 W. Szczerba, M. Schott, H. Riesemeier, A. F. Thunemann and D. G. Kurth, *Phys. Chem. Chem. Phys.*, 2014, **16**, 19694–19701.
11 Y. Tidhar, H. Weissman, S. G. Wolf, A. Gulino and B. Rybtchinski, *Chem.–Eur. J.*, 2011, **17**, 6068–6075.
12 F. Wurthner, C. C. You and C. R. Saha-Moller, *Chem. Soc. Rev.*, 2004, **33**, 133–146.
13 P. C. Griffiths, I. A. Fallis, T. Tatchell, L. Blishby and A. Beeby, *Adv. Colloid Interface Sci.*, 2008, **144**, 13–23.
14 F. Mancin, P. Scrimin, P. Tecilla and U. Tonellato, *Coord. Chem. Rev.*, 2009, **253**, 2150–2165.
15 Y. Qiao, Y. Y. Lin, Y. J. Wang, Z. Y. Yang, J. Liu, J. Zhou, Y. Yan and J. B. Huang, *Nano Lett.*, 2009, **9**, 4500–4504.
16 J. Zhang, X. G. Meng, X. C. Zeng and X. Q. Yu, *Coord. Chem. Rev.*, 2009, **253**, 2166–2177.
17 T. Owen and A. Butler, *Coord. Chem. Rev.*, 2011, **255**, 678–687.
18 Y. Qiao, Y. Y. Lin, S. Liu, S. F. Zhang, H. F. Chen, Y. J. Wang, Y. Yan, X. F. Guo and J. B. Huang, *Chem. Commun.*, 2013, **49**, 704–706.
19 C. Janiak, *Dalton Trans.*, 2003, 2781–2804.
20 S. Kitagawa, R. Kitaura and S. Noro, *Angew. Chem., Int. Ed.*, 2004, **43**, 2334–2375.
21 J. K. H. Hui and M. J. MacLachlan, *Coord. Chem. Rev.*, 2010, **254**, 2363–2390.
22 Y. Yan and J. B. Huang, *Coord. Chem. Rev.*, 2010, **254**, 1072–1080.
23 M. Du, C. P. Li, C. S. Liu and S. M. Fang, *Coord. Chem. Rev.*, 2013, **257**, 1282–1305.
24 M. L. Foo, R. Matsuda and S. Kitagawa, *Chem. Mater.*, 2014, **26**, 310–322.
25 L. M. Xu, L. X. Jiang, M. Drechsler, Y. Sun, Z. R. Liu, J. B. Huang, B. Z. Tang, Z. B. Li, M. A. C. Stuart and Y. Yan, *J. Am. Chem. Soc.*, 2014, **136**, 1942–1947.
26 N. T. Southall, K. A. Dill and A. D. J. Haymet, *J. Phys. Chem. B*, 2002, **106**, 521–533.
27 R. P. Sijbesma and E. W. Meijer, *Curr. Opin. Colloid Interface Sci.*, 1999, **4**, 24–32.
28 D. C. Sherrington and K. A. Taskinen, *Chem. Soc. Rev.*, 2001, **30**, 83–93.
29 H. Margenau, *Rev. Mod. Phys.*, 1939, **11**, 0001–0035.
30 Y. S. Zhao, H. B. Fu, A. D. Peng, Y. Ma, Q. Liao and J. N. Yao, *Acc. Chem. Res.*, 2010, **43**, 409–418.
31 F. S. Kim, G. Q. Ren and S. A. Jenekhe, *Chem. Mater.*, 2011, **23**, 682–732.
32 P. J. Stang and B. Olenyuk, *Acc. Chem. Res.*, 1997, **30**, 502–518.
33 G. F. Swiegers and T. J. Malefetse, *Chem. Rev.*, 2000, **100**, 3483–3537.
34 F. Wurthner, *Chem. Commun.*, 2004, 1564–1579.
35 K. Balakrishnan, A. Datar, T. Naddo, J. L. Huang, R. Oitker, M. Yen, J. C. Zhao and L. Zang, *J. Am. Chem. Soc.*, 2006, **128**, 7390–7398.
36 L. Zang, Y. K. Che and J. S. Moore, *Acc. Chem. Res.*, 2008, **41**, 1596–1608.
37 M. Huang, U. Schilde, M. Kumke, M. Antonietti and H. Colfen, *J. Am. Chem. Soc.*, 2010, **132**, 3700–3707.
38 D. Gorl, X. Zhang and F. Wurthner, *Angew. Chem., Int. Ed.*, 2012, **51**, 6328–6348.
39 G. H. Fu, M. L. Wang, Y. L. Wang, N. Xia, X. J. Zhang, M. Yang, P. Zheng, W. Wang and C. Burger, *New J. Chem.*, 2009, **33**, 784–792.
40 M. Ornatska, S. Peleshanko, B. Rybak, J. Holzmueller and V. V. Tsukruk, *Adv. Mater.*, 2004, **16**, 2206–2212.
41 K. Balakrishnan, A. Datar, W. Zhang, X. Yang, T. Naddo, J. Huang, J. Zuo, M. Yen, J. S. Moore and L. Zang, *J. Am. Chem. Soc.*, 2006, **128**, 6576.
42 M. H. Huang, U. Schilde, M. Kumke, M. Antonietti and H. Cölfen, *J. Am. Chem. Soc.*, 2010, **132**, 3700.
43 Y. Luo, J. Lin, H. Duan, J. Zhang and C. Lin, *Chem. Mater.*, 2005, **17**, 2234.
44 F. Würthner, *Chem. Commun.*, 2004, 1564.
45 G. B. Deacon and R. J. Phillips, *Coord. Chem. Rev.*, 1980, **33**, 227.
46 K. Nakamoto, *Infrared and Raman Spectra of Inorganic and Coordination Compounds*, Wiley, New York, 1997.